Intermetallics 183 (2025) 108830

Contents lists available at ScienceDirect

Intermetallics

journal homepage: www.elsevier.com/locate/intermet

Bauschinger effect on high entropy alloy under cyclic deformation

Hoang-Giang Nguyen [a,b,c], Sheng-Joue Young [b], Thanh-Dung Le [d], Thi-Nhai Vu [a,e], Te-Hua Fang [a,f,*]

[a] Department of Mechanical Engineering, National Kaohsiung University of Science and Technology, Kaohsiung, 807, Taiwan
[b] Department of Electronic Engineering, National United University, Miaoli City, Taiwan
[c] Faculty of Engineering, Kien Giang University, Kien Giang Province, Viet Nam
[d] Interdisciplinary Centre for Security, Reliability, and Trust (SnT), University of Luxembourg, Luxembourg
[e] Faculty of Mechanical Engineering, Nha Trang University, Khanh Hoa Province, Viet Nam
[f] Department of Fragrance and Cosmetic Science, Kaohsiung Medical University, Kaohsiung, 807, Taiwan

ARTICLE INFO

Keywords:
High-entropy alloys
Cyclic loading
Polycrystalline
Bauschinger effect
Fatigue life

ABSTRACT

This study employs molecular dynamics (MD) simulations to examine materials with comparable tension-compression behavior but markedly different cyclic fatigue performances. The findings reveal that the cyclic fatigue properties of AlCoCrCuFeNi high-entropy alloys (HEAs) are primarily governed by microscopic deformation mechanisms, particularly dislocation slip modes, which subtly affect initial work hardening. However, the slight initial differences in work hardening affected by the butterfly and Bauschinger effects gradually accumulate and intensify with repeated fatigue cycling. As the number of loading cycles increases, β-asymmetry steadily declines. Interactions between partial dislocations and stacking faults (SFs) at lower temperatures disrupt the lattice structure and impede dislocation reversal, thereby diminishing the Bauschinger effect. This mechanism contributes to marked variations in fatigue life and cyclic stress response.

1. Introduction

Structural components and their mechanical properties of high-entropy alloys have traditionally been designed based on monotonic loading characteristics. However, with the widespread occurrence of cyclic loading in real-world applications, fatigue-based design has garnered increasing attention in recent years [1]. Specifically, mitigating fatigue failure and accurately evaluating fatigue durability are critical tasks to prevent catastrophic failures and avoid economically significant breakdowns. These challenges are substantial in modern industries such as transportation, aerospace, energy, automotive, and oil [2]. Fatigue characterization of materials has typically relied on strain- or stress-controlled tests, which are both resource-intensive and time-consuming [3]. Consequently, there is a growing need for methods that can estimate fatigue properties or fatigue life through simpler and more efficient tests requiring minimal experimental effort [4]. A promising approach involves deriving fatigue characteristics from easily accessible monotonic mechanical data through basic tensile tests [2,5–7]. A long fatigue life is typically linked to high monotonic flexibility in the cyclic deformation regime [8,9]. However, exceptions to this trend exist. Previous studies have reported reduced low-cycle fatigue (LCF) resistance despite simultaneous increases in strength and flexibility in high-Mn steels [10]. Additionally, significant variations in LCF resistance have been observed in materials with comparable tensile properties [11], highlighting complex and ununderstood cyclic and monotonic deformation relationships.

This study employs molecular dynamics (MD) simulations to investigate the cyclic deformation behavior of AlCoCrCuFeNi high-entropy alloy (HEA), focusing on its microstructural evolution and stress-strain response. Cyclic deformation, as an extension of monotonic deformation, primarily reflects mechanical property changes in the initial strain stage. Consequently, evaluating cyclic properties based solely on macroscopic tensile strength or flexibility, as commonly done in prior studies [12–14], may lead to inaccuracies. Instead, microscopic damage mechanisms at low strains are the critical relationship between cyclic and monotonic deformation behaviors. The performance of cyclic deformation is susceptible to the dislocation slip mode, which can be inferred qualitatively from the work-hardening behavior observed during the initial phase of tensile deformation. This insight enables rapid and convenient estimation of cyclic deformation properties from partial

* Corresponding author. Department of Mechanical Engineering, National Kaohsiung University of Science and Technology, Kaohsiung, 807, Taiwan.
E-mail address: fang.tehua@msa.hinet.net (T.-H. Fang).

https://doi.org/10.1016/j.intermet.2025.108830
Received 3 January 2025; Received in revised form 22 April 2025; Accepted 12 May 2025
Available online 15 May 2025
0966-9795/© 2025 Elsevier Ltd. All rights are reserved, including those for text and data mining, AI training, and similar technologies.

tensile data, offering practical guidance for material selection and optimal design in engineering applications.

This study investigates the butterfly effect, Bauschinger effect, and the micro-mechanisms of AlCoCrCuFeNi under cyclic deformation. The paper is structured as follows: Section 2 details the MD modeling methods, Section 3 presents simulation results on the cyclic deformation of AlCoCrCuFeNi HEA while exploring the associated deformation mechanisms, and Section 4 summarizes the study's findings.

2. Methodologies

In this segment, we implemented the uniaxial cyclic tension-compression approach, illustrated in Fig. 1, followed by an evaluation of the outcomes to elucidate the plastic deformation properties of both single-crystal and polycrystalline AlCoCrCuFeNi High Entropy Alloy (HEA), as depicted in Fig. 1(c). Moreover, to scrutinize the impact of pre-existing grain boundaries on cyclic deformations, a model of polycrystalline AlCoCrCuFeNi HEA was constructed, as shown in Fig. 1(d).

The conjugate gradient algorithm aims to attain specimens characterized by minimal equilibrium energy and subsequently arrange the workpieces into a stable configuration preparatory to compressive and tensile loading scenarios [15,16]. A continuum of constant strain rates, including 10^8 s^{-1}, 5×10^8, 10^9, 5×10^9, and 10^{10} s^{-1}, encompass cyclic loading regimes along the x-axis. Cyclic loading incorporates a strain amplitude controlled at $\varepsilon = 0.15$. The models undergo relaxation for 200 ps at 300, 400, 500, 600, 700, 800, 900, and 1000 K to establish thermodynamic equilibrium, employing an isothermal-isobaric NPT ensemble before the loading phase [16,17]. The molecular dynamics simulation employs the NPT ensemble in the subsequent loading phase, utilizing a time step of 2 fs. The parameters in this study are presented in Table 1. The simulation process for the AlCoCrFeCuNi high-entropy alloy (HEA), as depicted in a previous study [18], consists of the following stages: Initially, atoms are randomly distributed within a face-centered cubic (FCC) lattice at 300 K. The system then undergoes a melting phase, during which atoms are gradually heated from 0.04 K/fs up to 1500 K while their velocities are adjusted to ensure thermal equilibrium at the maximum temperature. In the subsequent quenching stage, the system is rapidly cooled from 1500 K to 300 K, simulating environmental cooling, and then relaxed until thermal equilibrium is re-established at 300 K.

Molecular dynamics (MD) simulations in this study were performed using the open-source LAMMPS software [19,20]. Atomic interactions among Al, Co, Cr, Cu, Fe, and Ni were modeled using the embedded atom method (EAM) potential [21,22], and the results were analyzed and visualized with OVITO [23,24]. The von Mises shear strain was employed to characterize deformation evolution during tensile testing [25]. The atomic structures were identified via common neighbor analysis (CNA) [26], while dislocation structures were examined using the dislocation extraction algorithm (DXA) [27]. All simulations were executed in a constant temperature (NVT) ensemble, with temperature controlled by the Nose-Hoover thermostat.

Table 1
The simulation parameters under cyclic deformation.

Factor	Parameter
Materials type	AlCoCrCuFeNi
Size (nm)	300 (L) × 150 (W) × 35 (H)
Numbers of atoms	146200
Alloy composition	$Al_2Co_9Cr_{32}Cu_{39}Fe12Ni_6$
Strain rate (s^{-1})	1×10^9
Temperature	300, 400, 500, 600, 700, 800, 900, 1000

3. Results and discussion

Before the superalloys' microstructure evolution and mechanical properties under cyclic loading are investigated via simulations conducted at various ambient temperatures ranging from 300 K to 1000 K, all scenarios utilize a consistent strain rate of 10^9 s^{-1}, with ten cycles examined in each case. To facilitate analysis, each cycle is divided into four distinct phases: (I) $\varepsilon_1 = 0$ to 0.15 (Stage 1); (II) $\varepsilon_2 = 0.15$ to 0 (Stage 2, encompassing unloading and part of the reverse compressive phase); (III) $\varepsilon_3 = 0$ to -0.15 (Stage 3); and (IV) $\varepsilon_4 = -0.15$ to 0 (Stage 4, which involves unloading and some of the reverse tensile phase). Analysis of the results, as depicted in Fig. 2, reveals an initial occurrence of cyclic hardening attributed primarily to accumulating initial dislocations and stacking faults (SFs). Subsequently, the stress amplitude gradually stabilizes, reaching a state of cyclic saturation. The simulation outcomes suggest that the saturation state is achieved in fewer cycles than traditional fatigue experimental data, primarily due to the distinct time scale inherent in molecular dynamics (MD) simulation. Furthermore, it is observed that increasing temperature correlates with a reduction in the number of cycles required to attain cyclic saturation. Specifically, at lower temperatures of 300 K and 500 K, approximately ten cycles are needed for saturation, while at higher temperatures of 900 K and 1000 K, only around five cycles are required. This temperature dependency is attributed to decreased resistance to cross-slip at elevated temperatures, leading to accelerated hardening rates during the initial hardening stage.

Observations from Fig. 3 elucidate the conspicuous presence of surface features (SFs) on the sample. Within the temperature spectrum of 300 K–500 K, it is deduced within the temperature spectrum of 300 K–500 K that dislocations are the principal mechanism driving

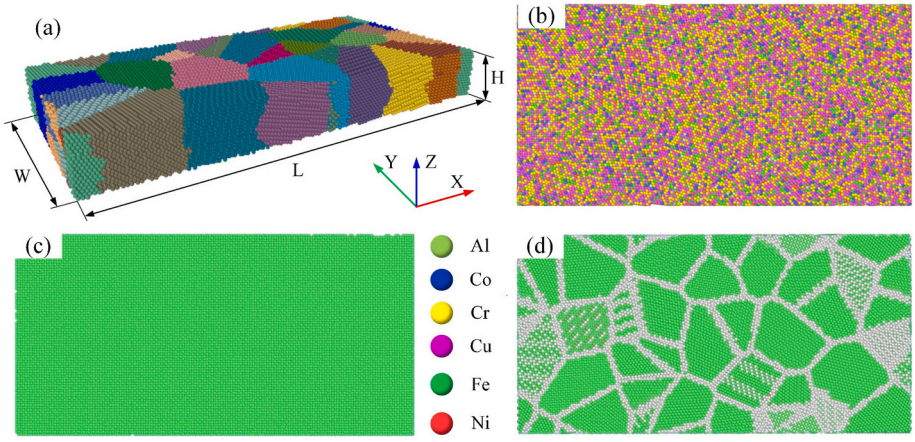

Fig. 1. Depicts an atomistic representation illustrating the response of high-entropy alloys to tension and compression loading, delineating distinct crystal structures. These structures are exemplified by (a) a single-crystal configuration and (b) a polycrystalline composition of AlCoCrCuFeNi HEAs.

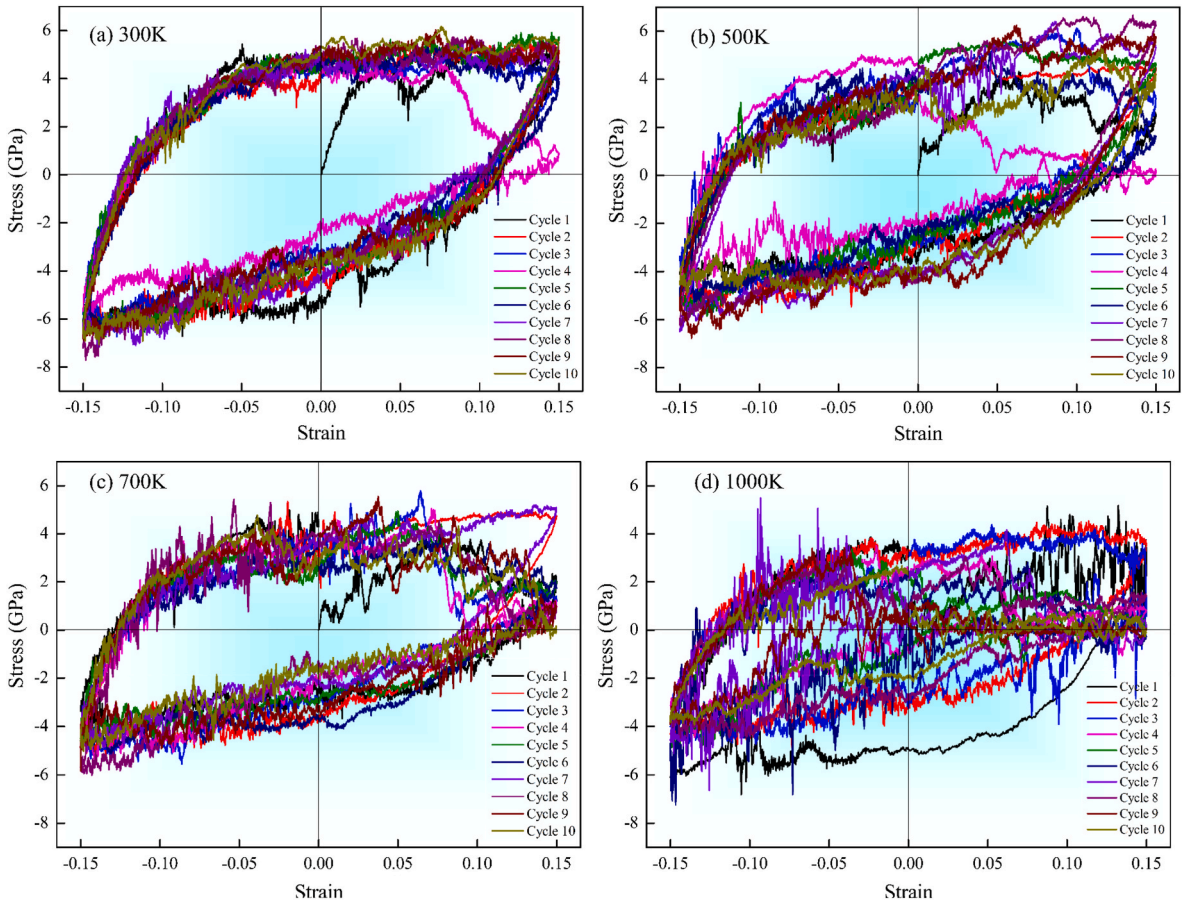

Fig. 2. The cyclic stress-strain curves at different temperatures with the strain rate of 10^9 s^{-1}.

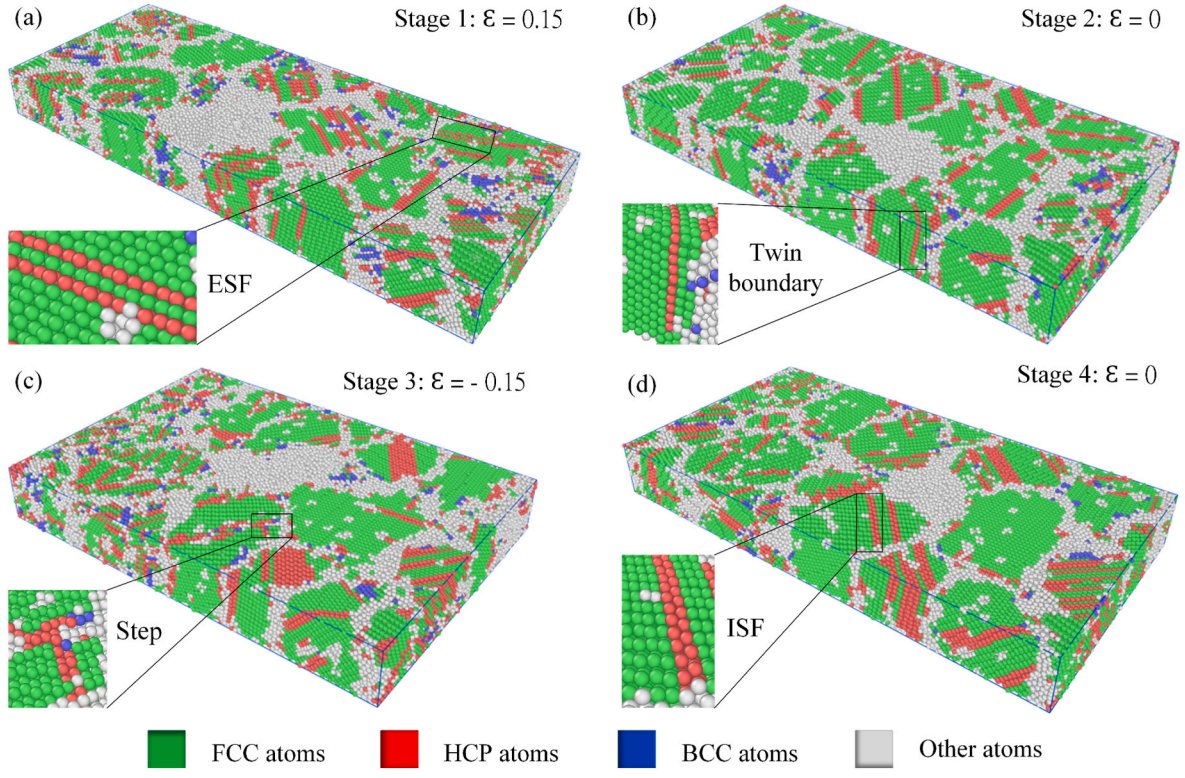

Fig. 3. Microstructure evolutions of AlCoCrCuFeNi HEA under cyclic deformation.

deformation. At the same time, SFs exhibit a persistent upward trend throughout the cyclic loading regimen. Conversely, as depicted in Fig. 3, escalating temperatures gradually diminish SFs on the surface, indicating a concurrent alteration in the alloy's deformation mechanism.

Fig. 4 illustrates the local stress distribution among atoms in AlCoCrCuFeNi high-entropy alloys (HEAs) with a grain size of 8.09 nm, subjected to cyclic deformation at a strain rate of 10^9 s^{-1}. The von Mises stress (VMS) values are used to color-code atoms based on local stress intensity. The VMS distribution varies significantly with temperature, strain rate, and deformation cycle. Notably, high-stress regions are consistently concentrated at the grain boundaries (GBs), where atomic density is inherently lower, leading to increased stress accumulation in these areas. Furthermore, plastic deformation expands with increasing temperature, particularly at 900 K and 1000 K, where elevated VMS values concentrate within GBs and internal grains, as illustrated in Fig. 4 (c and d). To quantitatively demonstrate this phenomenon, the percentage of atoms exhibiting VMS values exceeding 3.5 at $\varepsilon = 0.15$ is computed and presented in Fig. 4(a). Notably, a discernible increase in the proportion of atoms with high VMS values is observed with escalating temperatures, attributable to the heightened thermal vibration and kinetic energy of atoms at elevated temperatures.

The study delves into the atomic shear strain distribution within AlCoCrCuFeNi High Entropy Alloys (HEAs) with a characteristic grain size of d = 8.09 nm subjected to cyclic deformation, depicted in Fig. 5. Shear strain is a metric for evaluating the relative atomic displacement during cyclic loading, with atoms color-coded based on their shear strain values. Red denotes pronounced local deformation, and blue signifies minimal local deformation. Findings show that the initial deformation primarily occurs at grain boundaries (GB) due to their lower density. As plastic deformation progresses [28,29], intragranular shear bands emerge alongside pre-existing deformation near GBs, attributed to dislocation activity, as depicted in the cycle.

Notably, an increase in temperature reduces shear bands due to the amorphization process hindering stacking fault and twin boundary motion. Consequently, it suggests increased involvement of stacking faults, twin boundaries, and GB motion in plastic deformation. Furthermore, to elucidate the impact of temperature on atom motion or local deformation, the percentage of atoms with von Mises Shear Strain values exceeding 0.5 is computed, revealing a direct correlation between elevated temperatures and a higher fraction of atoms exhibiting significant VMSS induced by cyclic activation, as illustrated in Fig. 5(d).

Fig. 6. Cross-sectional view (x-z plane) of the dislocations AlCoCrCuFeNi with the mean grain size of 8.09 nm using the DXA in the (a) forward tension-deformed sample up to the strain of $\varepsilon = 0.15$, (b) reverse compression-deformed sample up to the strain of $\varepsilon = 0$, (c) compression-deformed sample up to the strain of $\varepsilon = -0.15$, and (d) alteration in dislocation density with simulation time in a reverse compression-deformed sample up to the strain of $\varepsilon = 0$. The detwinning process is effectively elucidated through computational techniques, notably the (DXA) [30], incorporated within the OVITO visualization software to analyze atomistic simulations. The DXA facilitates the identification of dislocations, determination of their Burgers vectors, and localization of dislocation lines within crystals. The dislocation distribution across un-deformed, forward tension-deformed, and reverse compression-deformed samples is depicted in Fig. 6. Initial tensile deformation initiates dislocation activity within select grains, leading to a subsequent increase in dislocation density. Analysis of the Burgers vectors identifies five distinct dislocation types in the deformed atomic structure: Shockley partial dislocations (1/6⟨112⟩), perfect dislocations (⟨110⟩), Frank dislocations (1/2⟨111⟩), stair-rod dislocations (1/6⟨110⟩), and Hirth dislocations (1/3⟨001⟩), represented by green, blue, cyan, pink, and yellow lines in Fig. 6, respectively. Additional unidentified dislocations, labeled as other dislocations in Fig. 6(d), are also observed. Among these, Shockley partial dislocations, perfect dislocations, and other dislocations are predominant. Under forward tensile loading up to a strain of $\varepsilon = 0.15$, Shockley partial dislocations exhibit rapid growth in length, eventually becoming the dominant dislocation type [31]. Conversely, during reverse-compression deformation up to a total strain of $\varepsilon = 0$, the length of Shockley partial dislocations diminishes significantly while the lengths of perfect and other dislocations increase.

Fig. 7(a). Presents a comprehensive analysis of the impact of strain rates on dislocation evolution. It reveals a pattern wherein the dislocation length exhibits periodic increments and decrements throughout cyclic loading. The total dislocation length initially undergoes regular fluctuations from the onset until reaching the yield point. Subsequently, notable changes in dislocation length occur, with a significant increase observed during stage I of cycle 1, followed by a slight decrease in stage II and a minor rise in stage III of the same cycle. At the initial cycle, a consistent pattern emerges wherein the total dislocation length experiences increases and decreases in correspondence with each cycle stage.

Overall, a discernible increasing trend in total dislocation length with successive cycles is observed, suggesting a significant influence of cyclic loading on the mechanical properties and deformation evolution of the AlCoCrCuFeNi HEAs alloy during cyclic deformation testing. However, it is noted that while the cycle exerts an influence, its impact is comparatively lesser than that of other factors, such as temperature and strain rate, albeit more significant than that of grain size.

Increased lattice disorder hinders dislocation reverse glide, reducing the Bauschinger effect. The β-asymmetry value is obtained by quantitatively averaging the stress ratios just before unloading and the yielding stress of the subsequent reverse loading across all total load cycles to

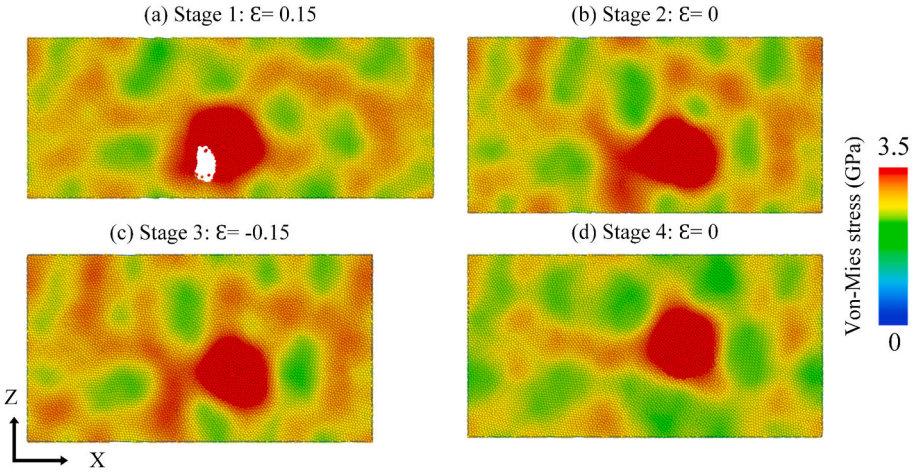

Fig. 4. The von Mises allocation of AlCoCrCuFeNi models under the cyclic deformation process.

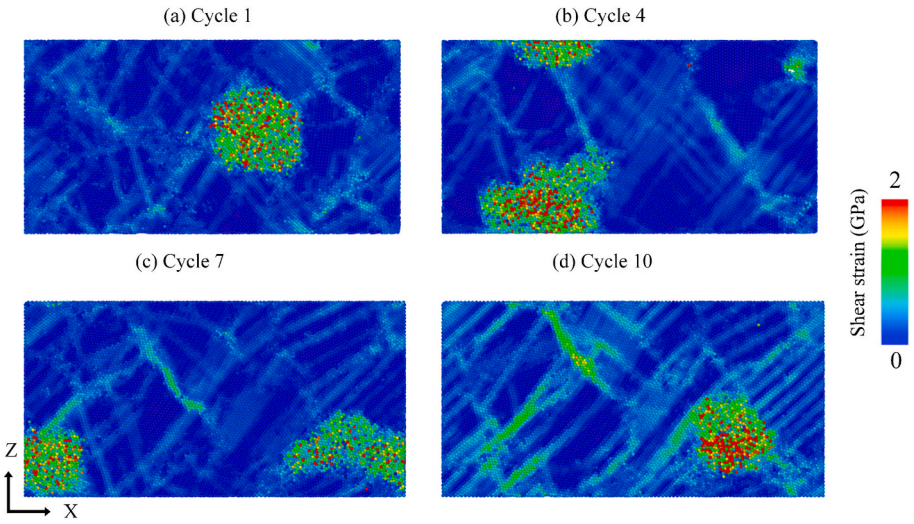

Fig. 5. The shear strain of AlCoCrCuFeNi models under the cyclic deformation process.

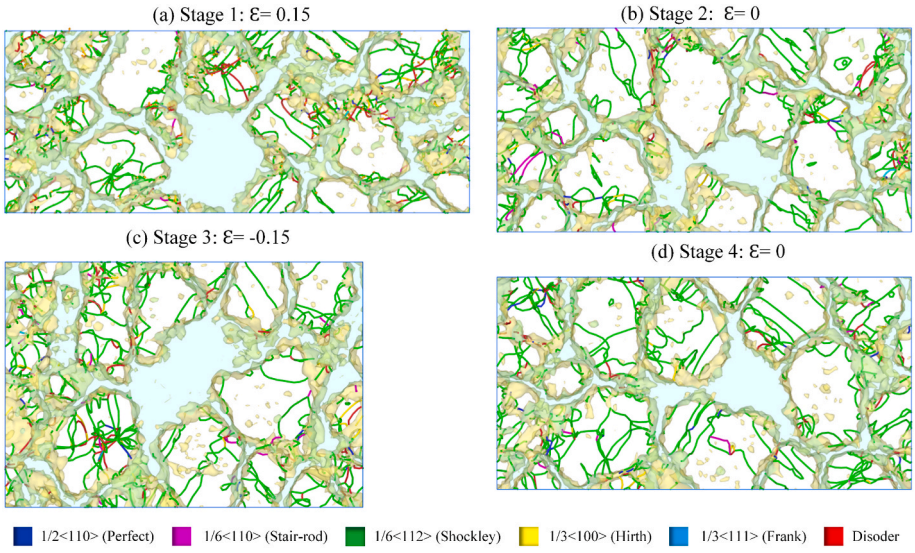

Fig. 6. Dislocation extraction algorithm (DXA) of AlCoCrCuFeNi HEA for under cyclic deformation.

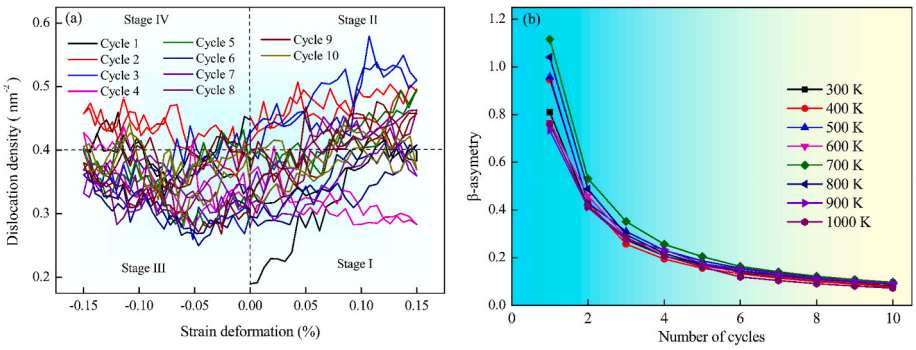

Fig. 7. Total dislocation density of AlCoCrCuFeNi HEAs under cyclic deformation (a). The average β-asymmetry value at various temperatures during cyclic loading (b).

assess the Bauschinger effect [9,32].

$$\beta\text{-asymmetry} = \sum_{i=1}^{n} \left| \frac{\sigma_i^+}{\sigma_i^-} \right| \Big/ n \quad (1)$$

Where σ_i^+ and σ_i^- denote the stress immediately before unloading and the corresponding yield stress reversal during the ith loading phase, respectively, while n denotes the total number of cycles. According to this definition, a more prominent B-asymmetry factor suggests a more

significant Bauschinger effect throughout the loading cycle. Since cyclic loading involves two unloading stages, both components of the β-asymmetry are determined for stages II and IV. The average β-asymmetry rate of the AlCoCrCuFeNi HEA during cyclic deformation at different temperatures is presented in Fig. 7 b. The graph depicts the relationship between β-asymmetry and the number of loading cycles across temperatures ranging from 300 K to 1000 K. β-asymmetry exhibits a nonlinear decline with increasing cycles, characterized by a sharp initial drop followed by gradual stabilization. While initial β-asymmetry values are relatively high at all temperatures, they converge toward a similar lower bound after approximately 8–10 cycles. Notably, at lower temperatures (300 K), the initial β-asymmetry is slightly lower than at higher temperatures (700 K). However, despite variations in initial values, the trend across all temperatures consistently demonstrates a rapid reduction followed by stabilization, suggesting that the effect of temperature on β-asymmetry diminishes as the cyclic deformation progresses. The influence of temperature on the formation of lattice disorder in HEAs under cyclic loading exhibits a trend similar to that shown in Fig. 6. These factors help inhibit dislocation reversal, thereby reducing the Bauschinger effect. The effect of temperature on the development of HEA lattice disorder under cyclic loading mirrors the pattern observed in Fig. 6. It helps prevent dislocations from moving in reverse and increases σ_i^-, thereby reducing the Bauschinger effect.

Table 2 provides data on the β-asymmetry and the distribution of crystal structures in AlCoCrCuFeNi high-entropy alloy (HEA) at 300 K under cyclic loading. The β-asymmetry decreases steadily with the number of loading cycles, from 0.8096 in Cycle 1 to 0.0825 in Cycle 10. The percentage remains relatively constant for the body-centered cubic (BCC) phase, fluctuating slightly between 2.1 % and 3.5 % across cycles. The face-centered cubic (FCC) phase initially increases, reaching a peak of 54.8 % in Cycle 6 before slightly declining to 50.3 % in Cycle 10. The hexagonal close-packed (HCP) phase gradually rises, starting at 14.1 % in Cycle 1 and reaching 20 % by Cycle 10. Meanwhile, the proportion of other structures decreases from 36.4 % in Cycle 1–27.6 % in Cycle 10, reflecting a redistribution of phases under cyclic loading. This progression illustrates the evolving microstructural dynamics of the alloy during cyclic deformation.

Table 3 provides a comparative analysis of various parameters obtained from molecular dynamics (MD) simulations and experimental investigations. It includes data for different materials, such as AlCoCrCuFeNi and CoCuFeMnNi, characterized by strain rate, temperature, strain, stress, cycle, and method. For AlCoCrCuFeNi, the strain rate varies from 10^8 to 10^{10} s^{-1}, with temperatures ranging between 300 and 1000 K, producing strains of 15–20 % and stress values between 3.95 and 15.14 GPa. These values were derived through MD simulations as reported in multiple references, including the current study and previous works by Vu et al. [7] and Nguyen et al. [9] studies, such as Ma et al. [6] investigation reported a strain rate of 10^{-3} to 3×10^3 s^{-1}, strain of 30 %, and stress of 2.123 GPa. In comparison, CoCuFeMnNi exhibited a strain rate range of 10^{-3} to 5×10^{-3} s^{-1}, a temperature of 1273 K, strain of 0.5–1.5 %, and stress of 0.71 GPa, derived experimentally by Bahadur et al. [32] Notably, the cycle parameter is limited to 10 cycles for MD simulations, while experimental investigations of CoCuFeMnNi reached up to 2×10^4 cycles. These findings highlight the differences in methodologies and conditions between simulations and experiments for evaluating mechanical properties.

Table 2
The β-asymmetry and crystal structure percentages in AlCoCrCuFeNi HEA at 300 K under cyclic loading.

Cycle	β-asymmetry	BCC (%)	FCC (%)	HCP (%)	Other (%)
1	0.8096	3.5	46.1	14.1	36.4
2	0.4140	3.3	51.5	15.3	29.9
3	0.2753	2.2	49.2	16.5	32.1
4	0.2077	2.7	45.3	18.6	33.4
5	0.1681	2.2	51.8	15.1	30.9
6	0.1394	2.2	54.8	15.5	27.5
7	0.1178	2.5	48.7	18.6	30.2
8	0.1016	2.2	54.6	16.6	26.6
9	0.0911	2.1	53.7	18.7	25.6
10	0.0825	2.2	50.3	20	27.6

4. Conclusions

In summary, this study explored the effects of the Bauschinger effect and butterfly effect on the mechanical behavior of AlCoCrCuFeNi HEA under cyclic deformation using MD simulations. The key findings are summarized as follows:

(1) The molecular dynamics simulations of uniaxial cyclic loading reveal an imbalance between tension and compression.
(2) The AlCoCrCuFeNi HEA demonstrates strain rates of 10^8–10^{10} s^{-1}, temperatures between 300 and 1000 K, strains of 15–20 %, and corresponding stress levels from 3.95 to 15.14 GPa.
(3) The β-asymmetry decreases steadily with the number of loading cycles. Additionally, polycrystallinity can destabilize the FCC structure, increase lattice disorder, hinder dislocation reversal, and reduce the Bauschinger effect under cyclic loading.
(4) The SFE of the HEA decreases with lower temperatures, promoting partial dislocations and more significant SF regions. The interaction between partial dislocations and SFs induces lattice disorder and hinders dislocation reversal, weakening the Bauschinger effect at lower temperatures.

This study provides insights into the atomic mechanisms governing cycle plasticity in AlCoCrCuFeNi HEA, the evolution of microstructures under cyclic deformation, and the role of lattice disorder in the Bauschinger effect. However, the Bauschinger effect and its underlying mechanisms may differ in high-entropy alloys (HEAs) containing grain boundaries, especially in specimens with larger grain sizes. Future studies should systematically explore the cyclic plasticity behavior of polycrystalline HEAs.

CRediT authorship contribution statement

Hoang-Giang Nguyen: Writing – review & editing, Writing – original draft, Visualization, Validation, Software, Investigation, Formal analysis, Data curation, Conceptualization. **Sheng-Joue Young:** Writing – review & editing, Supervision, Resources, Project administration, Methodology, Funding acquisition. **Thanh-Dung Le:** Writing – review & editing, Visualization, Validation, Investigation, Formal analysis. **Thi-Nhai Vu:** Writing – review & editing, Investigation, Formal analysis. **Te-Hua Fang:** Writing – review & editing, Supervision, Software, Resources, Project administration, Methodology, Funding acquisition, Formal analysis.

Prime novelty statement

As the corresponding author, I, Te-Hua Fang, confirm on behalf of all authors that the manuscript titled “Bauschinger Effect on High Entropy Alloy under Cyclic Deformation” presents the following novel findings:

✓Molecular dynamics simulations of uniaxial cyclic loading reveal asymmetry between tensile and compressive responses.
✓ The β-asymmetry decreases with cycling, as polycrystallinity disrupts FCC stability and diminishes the Bauschinger effect.
✓ The stacking fault energy (SFE) of the HEA decreases with lower temperatures, promoting partial dislocations and stacking fault regions. Interactions between partial dislocations and stacking faults induce lattice disorder, hinder dislocation reversals, and reduce the Bauschinger effect.

Table 3
The comparison some of value between this investigations in this study with others.

Material	Strain rate (s^{-1})	Temperature (K)	Strain (%)	Stress (GPa)	Cycle	Method	Reference
AlCoCrCuFeNi	10^8–10^{10}	300–1000	15	5.49	10	MD Simulation	This study
$AlCoCrFeNi_{2.1}$	$10^{-3} - 3 \times 10^3$	298–1823	60	1.86	–	Experimental	Hu et al. [6]
AlCoCrFeNi	10^8–10^{10}	300–1100	20	3.95	–	MD Simulation	Vu et al. [7]
AlCrCuFeNi	10^8–10^{10}	300–1100	15	14.93	10	MD Simulation	Nguyen et al. [9]
AlCrCuFeNi	10^8–10^{10}	300	20	15.14	–	MD Simulation	Doan et al. [16]
CoCuFeMnNi	10^{-3} -5 $\times$ 10^{-3}	1273	0.5-1.5	0.71	2×10^4	Experimental	Bahadur et al. [32]

These findings mark the first comprehensive study of the Bauschinger and butterfly effects under cyclic deformation in AlCoCrCuFeNi high-entropy alloys.

Declaration of competing interest

The authors declare that they have no known competing financial interests or personal relationships that could have appeared to influence the work reported in this paper.

Acknowledgments

The authors acknowledge the support by the National Science and Technology Council, Taiwan, under grant numbers NSTC 113-2221-E-992-067-MY3, NSTC 113-2811-E239-002, and Industry Cooperation Project no. 113A00262.

Data availability

The authors do not have permission to share data.

References

[1] D. Jeddi, T. Palin-Luc, A review about the effects of structural and operational factors on the gigacycle fatigue of steels, Fatig. Fract. Eng. Mater. Struct. 41 (5) (2018) 969–990, https://doi.org/10.1111/ffe.12779.
[2] C.W. Shao, P. Zhang, R. Liu, Z.J. Zhang, J.C. Pang, Z.F. Zhang, Low-cycle and extremely-low-cycle fatigue behaviors of high-Mn austenitic TRIP/TWIP alloys: property evaluation, damage mechanisms, and life prediction, Acta Mater. 103 (2016) 781–795, https://doi.org/10.1016/j.actamat.2015.11.015.
[3] B. Adamczyk-Cieślak, M. Koralnik, R. Kuziak, T. Brynk, T. Zygmunt, J. Mizera, Low-cycle fatigue behaviour and microstructural evolution of pearlitic and bainitic steels, Mater. Sci. Eng., A 747 (2019) 144–153, https://doi.org/10.1016/j.msea.2019.01.043.
[4] X.Y. Long, R. Branco, F.C. Zhang, F. Berto, R.F. Martins, Influence of Mn addition on cyclic deformation behaviour of bainitic rail steels, Int. J. Fatig. 132 (2020) 105362, https://doi.org/10.1016/j.ijfatigue.2019.105362.
[5] H.G. Nguyen, T.D. Le, H.G. Nguyen, T.H. Fang, Mechanical properties of AlCoCrCuFeNi high-entropy alloys using molecular dynamics and machine learning, Mater. Sci. Eng. R Rep. 160 (2024) 100833, https://doi.org/10.1016/j.mser.2024.100833.
[6] M. Hu, K. Song, W. Song, Dynamic mechanical properties and microstructure evolution of AlCoCrFeNi2. 1 eutectic high-entropy alloy at different temperatures, J. Alloys Compd. 892 (2022) 162097, https://doi.org/10.1016/j.jallcom.2021.162097.
[7] T.N. Vu, V.T. Pham, T.H. Fang, Influences of grain size, temperature, and strain rate on mechanical properties of Al0. 3CoCrFeNi high–entropy alloys, Mater. Sci. Eng., A 858 (2022) 144158, https://doi.org/10.1016/j.msea.2022.144158.
[8] H. Mughrabi, H.W. Höppel, M. Kautz, Fatigue and microstructure of ultrafine-grained metals produced by severe plastic deformation, Scr. Mater. 51 (8) (2004) 807–812, https://doi.org/10.1016/j.scriptamat.2004.05.012.
[9] H.G. Nguyen, T.H. Fang, D.Q. Doan, Cyclic plasticity and deformation mechanism of AlCrCuFeNi high entropy alloy, J. Alloys Compd. 940 (2023) 168838, https://doi.org/10.1016/j.jallcom.2023.168838.
[10] C.W. Shao, P. Zhang, R. Liu, Z.J. Zhang, J.C. Pang, Q.Q. Duan, Z.F. Zhang, A remarkable improvement of low-cycle fatigue resistance of high-Mn austenitic TWIP alloys with similar tensile properties: importance of slip mode, Acta Mater. 118 (2016) 196–212, https://doi.org/10.1016/j.actamat.2016.07.034.
[11] S. Picak, T. Wegener, S.V. Sajadifar, C. Sobrero, J. Richter, H. Kim, I. Karaman, On the low-cycle fatigue response of CoCrNiFeMn high entropy alloy with ultra-fine grain structure, Acta Mater. 205 (2021) 116540, https://doi.org/10.1016/j.actamat.2020.116540.
[12] D.R. Abashev, V.S. Bondar, Modified theory of plasticity for monotonic and cyclic deformation processes, Mech. Solid. 56 (1) (2021) 4–12, https://doi.org/10.3103/S0025654421010027.
[13] D. Abashev, V. Bondar, Refinement of plasticity theory for modeling monotonic and cyclic loading processes, J. Mech. Mater. Struct. 15 (2) (2020) 225–239, http://10.0.8.92/jomms.2020.15.225.
[14] V.S. Bondar, D.R. Abashev, Mathematical modeling of the monotonic and cyclic loading processes, Strength Mater. 52 (3) (2020) 366–373, https://doi.org/10.1007/s11223-020-00186-7.
[15] J. Li, Q. Fang, B. Liu, Y. Liu, Y. Liu, Atomic-scale analysis of nanoindentation behavior of high-entropy alloy, J. Micromech. Mole. Phys. 1 (1) (2016) 1650001, https://doi.org/10.1142/S2424913016500016.
[16] D.Q. Doan, T.H. Fang, T.H. Chen, T.X. Bui, Effects of void and inclusion sizes on mechanical response and failure mechanism of $AlCrCuFeNi_2$ high-entropy alloy, Eng. Fract. Mech. 252 (2021) 107848, https://doi.org/10.1016/j.engfracmech.2021.107848.
[17] Z. Wang, J. Li, Q. Fang, B. Liu, L. Zhang, Investigation into nanoscratching mechanical response of AlCrCuFeNi high-entropy alloys using atomic simulations, Appl. Surf. Sci. 416 (2017) 470–481, https://doi.org/10.1016/j.apsusc.2017.04.009.
[18] J. Li, Q. Fang, B. Liu, Y. Liu, Y. Liu, Mechanical behaviors of AlCrFeCuNi high-entropy alloys under uniaxial tension via molecular dynamics simulation, RSC Adv. 6 (80) (2016) 76409–76419, https://doi.org/10.1039/C6RA16503F.
[19] H.G. Nguyen, T.H. Fang, Machining mechanism and residual stress of AlCuCrFeNi alloy, Int. J. Mech. Sci. (2024) 109429, https://doi.org/10.1016/j.ijmecsci.2024.109429.
[20] H. Xu, Y. Xiao, G. Yu, Z. He, Z. Hai, Molecular dynamics study on transport process of membrane separation for carbon dioxide capture, Comput. Mater. Sci. 244 (2024) 113233, https://doi.org/10.1016/j.commatsci.2024.113233.
[21] M.S. Daw, S.M. Foiles, M.I. Baskes, The embedded-atom method: a review of theory and applications, Mater. Sci. Rep. 9 (7–8) (1993) 251–310, https://doi.org/10.1016/0920-2307(93)90001-U.
[22] D. Utt, A. Stukowski, K. Albe, Grain boundary structure and mobility in high-entropy alloys: a comparative molecular dynamics study on a Σ11 symmetrical tilt grain boundary in face-centered cubic CuNiCoFe, Acta Mater. 186 (2020) 11–19, https://doi.org/10.1016/j.actamat.2019.12.031.
[23] A. Stukowski, Visualization and analysis of atomistic simulation data with OVITO–the Open Visualization Tool, Model. Simulat. Mater. Sci. Eng. 18 (1) (2009) 015012. https://doi10.1088/0965-0393/18/1/015012.
[24] H.G. Nguyen, T.H. Fang, Mechanics of AlCuNiTi alloy orthogonal micro-cutting, Model. Simulat. Mater. Sci. Eng. 31 (8) (2023) 085016. https://doi10.1088/1361-651X/ad064f.
[25] A.V. Pham, T.H. Fang, A.S. Tran, T.H. Chen, Structural and mechanical characterization of sputtered CuxNi100-x thin film using molecular dynamics, J. Phys. Chem. Solid. 147 (2020) 109663, https://doi.org/10.1016/j.jpcs.2020.109663.
[26] J.D. Honeycutt, H.C. Andersen, Molecular dynamics study of melting and freezing of small Lennard-Jones clusters, J. Phys. Chem. 91 (19) (1987) 4950–4963, https://doi.org/10.1021/j100303a014.
[27] Y. Qi, H. Xu, T. He, M. Wang, M. Feng, Atomistic simulation of deformation behaviors polycrystalline CoCrFeMnNi high-entropy alloy under uniaxial loading, Int. J. Refract. Metals Hard Mater. 95 (2021) 105415, https://doi.org/10.1016/j.ijrmhm.2020.105415.
[28] P. Ranjan, A. Owhal, D. Chakrabarti, S.U. Belgamwar, T. Roy, R. Balasubramaniam, Fundamental insights of mechanical polishing on polycrystalline Cu through molecular dynamics simulations, Mater. Today Commun. 32 (2022) 103980, https://doi.org/10.1016/j.mtcomm.2022.103980.
[29] H. Ghaffarian, A.K. Taheri, K. Kang, S. Ryu, Molecular dynamics simulation study of the effect of temperature and grain size on the deformation behavior of polycrystalline cementite, Scr. Mater. 95 (2015) 23–26, https://doi.org/10.1016/j.scriptamat.2014.09.022.
[30] A. Stukowski, K. Albe, Extracting dislocations and non-dislocation crystal defects from atomistic simulation data, Model. Simulat. Mater. Sci. Eng. 18 (8) (2010) 085001. https://doi10.1088/0965-0393/18/8/085001.
[31] R. Mohammadzadeh, Reversible deformation in nanocrystalline TWIP steel during cyclic loading by partial slip reversal and detwinning, Mater. Sci. Eng., A 782 (2020) 139251, https://doi.org/10.1016/j.msea.2020.139251.
[32] F. Bahadur, K. Biswas, N.P. Gurao, Micro-mechanisms of microstructural damage due to low cycle fatigue in CoCuFeMnNi high entropy alloy, Int. J. Fatig. 130 (2020) 105258, https://doi.org/10.1016/j.ijfatigue.2019.105258.